Materials Research Proceedings 28 (2023) 1223-1234 https://doi.org/10.21741/9781644902479-133

# Modeling of surface hardening in burnishing process

TEIMOURI Reza[1,a *], GRABOWSKI Marcin[1,b] and SKOCZYPIEC Sebastian[1,c]

[1] Cracow University of Technology, Faculty of Mechanical Engineering, Chair of Production Engineering, al. Jana Pawła II 37, 31-864, Kraków, Poland

[a]reza.teimouri@pk.edu.pl, [b]marcin.grabowski@pk.edu.pl, [c]sebastain.skoczypiec@pk.edu.pl

**Keywords:** Burnishing, Twining-Induced Hardening, Phase Change, Simulation

**Abstract.** In the present paper, a multiphysic model was developed to identify the underlying mechanism of surface layer hardening in burnishing of stainless steel 304. The mechanic of burnishing process was firstly modeled to obtain deformation parameters i.e. strain and strain rate by incremental plasticity. Then the strengthening mechanisms were identified association of constitutive equations regarding twinning-induced hardening and phase change. It was found that the twining-induced hardening has greatest contribution in strengthening the surface layer. Moreover, among the process parameters, the burnishing depth has greatest effect on hardness magnitude and corresponding depth.

## Introduction

Burnishing is categorized as surface finishing operations which are being used for surface smoothening, and mechanical properties enhancement of the engineering materials [1,2]. Compared to other mechanical surface treatment processes such as shot peening, laser shock peening, or ultrasonic peening, burnishing results in better surface quality and induces compressive residual stress at deeper layers [3]. Moreover, it is easily implemented and does not require complex instrumentations and machines. Thus, it is finding its importance at industrial levels such as aerospace and automotive for the superfinishing of hard materials.

During burnishing, the microstructure evolution is corresponded to different microstructure phenomena that can result in hardening of burnished surface layer. However, in majority of conducted research, the underlying mechanism of surface strengthening has been reported as grain refinement Based on the type of material, hardening mechanisms such as dislocation accumulation, crystal twinning and phase change can be also effective in strengthening of surface layer. Starman et al. [4] reported that the martensitic phase transformation corresponds to the surface hardening of AISI 304 processed by shot-peening and laser shock peening. Laine et al. [5] revealed that the twining-induced hardening beside grain size evolution has contribution in surface hardening of shot-peened Ti64 alloy. Rinaldi et al. [6] identified that the strengthening mechanism of CP-T alloy in hard machining process is mainly attributed to twining induced plasticity and grain refinement.

In order to identify the main strengthening mechanism, complex microscopic examination and mechanical testing is required. However, providing such examination techniques for considerable amount of experiments are too expensive and time consuming. In this context, development of material model based on multiphysics of different metallurgical phenomena can be considered as a fundamental means to afford the lack of capabilities of measurement instrumentation and to identify the underlying mechanisms.

In the present study, a theoretical approach based on multiphysics of contact mechanic and multiscale micro-mechanical material model is developed to identify the underlying strengthening mechanism AISI 304 samples processed by burnishing process. Here, firstly the deformation parameters of process like stress, strain and strain rate are modeled by expanding cavity model. Then the strengthening mechanisms are identified by developing a material model including grain

refinement, twinning-induced hardening and phase change. Confirmation of developed theoretical model has been carried out by series of burnishing experiments including different processing parameters.

**Theoretical model**

Deformation parameter.

Fig. 1 illustrates the schematic diagram of the rolling of a roller on the flat surface that is the main concept of roller burnishing process. In order to calculate the deformation parameters, theory of expanded cavity model (ECM) proposed by Gao et al. [7] utilized here. Accordingly, the mean contact pressure applied by burnishing roller to the surface of the power law hardening material can be calculated by following equation:

$$p_m = \frac{\sigma_y}{\sqrt{3}}\left[1 + \frac{1}{n}\left(\frac{r_p^{2n}}{a^{2n}} - 1\right)\right] + k\varepsilon_{eq}^{n} \tag{1}$$

where $r_e$, $n$ and $k$ are, respectively, the outer radius of cylinder, strain hardening exponent and material constant for power law. Also, $r_p$ and $\varepsilon_{eq}$ are the the plastic boundary of deformation and equivalant plastic strain of contact which can be calculated by following formulation [8].

$$\varepsilon_{eq} = \sqrt{6}\frac{\sigma_y}{E}\frac{r_p^2}{r^2} \quad , \quad r_p = \sqrt{\frac{2Ea^3}{\sqrt{3}R\sigma_y}} \tag{2}$$

Once the mean contact pressure is identified, the burnishing force of an each individual roller induces to a surface can be obtained by following formula:

$$F = 2aLp_m \, , \; a = \sqrt{2R\delta} \tag{3}$$

where $L$ is roller length, $a$ is the penetration radius and $\delta$ is the burnishing depth.

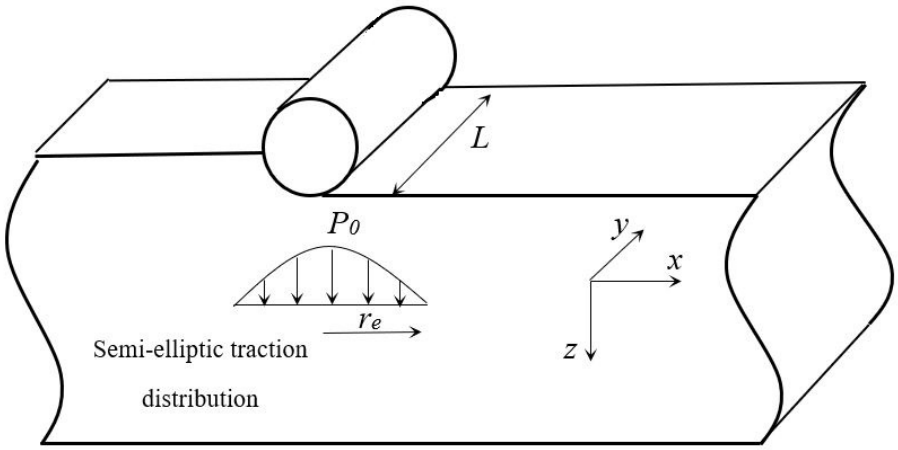


*Fig. 1. Schematic illustration of contact of a cylindrical roller to flat surface.*

In order to calculate the deformation parameters during motion of the roller over the surface, the theory of incremental plasticity for rolling contact that is suggested by McDowel is utilized [9]. Based on this theory, the loading initiates by elastic stresses and it incrementally increases up to reaching plastic region. Finally, by moving the tool too far from the point of interest, the unloading occurs. The elastic stresses at point of interest *M(x,z)* can be calculated using integration

of Boussineq solution for the normal traction *p(s)* and tangential traction *q(s)* in semi-infinite half space over the region of contact [10].

$$\begin{cases} \sigma_{xx}(x,z) = -\dfrac{2z}{\pi}\int_{-a}^{a}\dfrac{p(s)(x-s)^2}{[(x-s)^2+z^2]^2}ds - \dfrac{2}{\pi}\int_{-a}^{a}\dfrac{q(s)(x-s)^3}{[(x-s)^2+z^2]^2}ds \\ \sigma_{zz}(x,z) = -\dfrac{2z^3}{\pi}\int_{-a}^{a}\dfrac{p(s)}{[(x-s)^2+z^2]^2}ds - \dfrac{2z^2}{\pi}\int_{-a}^{a}\dfrac{q(s)(x-s)}{[(x-s)^2+z^2]^2}ds \\ \tau_{xz}(x,z) = -\dfrac{2z^2}{\pi}\int_{-a}^{a}\dfrac{p(s)(x-s)}{[(x-s)^2+z^2]^2}ds - \dfrac{2z}{\pi}\int_{-a}^{a}\dfrac{q(s)(x-s)^2}{[(x-s)^2+z^2]^2}ds \end{cases} \tag{4}$$

More specifically, by assuming semi-elliptic distribution of tangential and normal traction based on boussinesque formulation, following relationship between the axial and tangential tractions and burnishing force are established.

$$p(s) = \frac{F}{a}\sqrt{1-\left(\frac{2s}{a}-1\right)^2}\ ,\ q(s) = \frac{\mu F}{a}\sqrt{1-\left(\frac{2s}{a}-1\right)^2} \tag{5}$$

By identifying the values of elastic stresses, the elastic strain can be obtained using Hook's law taking into account the plain strain condition i.e. $\varepsilon_{yy}=0$.
In order to calculate the value of plastic stress and strains at any individual poit, the yielding criteria by comparing the value of effective stress and Johnson-Cook constitutive model is identified as follows:

$$\begin{cases} g = \dfrac{1}{2}(S_{ij}-a_{ij})(S_{ij}-a_{ij}) - Y^2 \\ Y = \dfrac{1}{\sqrt{3}}(A + B{\varepsilon_{eff}}^n)\left[1 + C\ln\left(\dfrac{\dot{\varepsilon}_{eff}}{\dot{\varepsilon}_0}\right)\right]\left(\dfrac{T-T_0}{T_m-T_0}\right)^m \\ S_{ij} = \sigma_{ij} - \dfrac{1}{3}\delta_{ij}\sigma_{kk} \end{cases} \tag{6}$$

where $S_{ij}$ is deviatoric stress, and $a_{ij}$ is back stress tensors. Also, $Y$ is the effective stress based on Johnson-Cook (J-C) yield criterion. $A$, $B$ and $C$ are the *J-C* constants, $\varepsilon_{eff}$ and $\dot{\varepsilon}_{eff}$ are effective strain and effective strain rate, respectively, which are calculated based on incremental plasticity theory that will be described in following part. Furthermore, $T$ is the temperature term which can be neglected in burnishing process [11]. According to Eq. 6, when the g>0, the loading at the point of interest is elastic, and the stress and strain can be calculated using Eq. 4, and Hook's law. When g>0, the plastic loading occurs, and to obtain values of plastic strain and stress, the systems of three equations suggested by McDowel need to be solved.

$$\begin{cases} d\varepsilon_{xx} = \dfrac{1}{E}\left[d{\sigma_{xx}}^p - \vartheta\left(d{\sigma_{yy}}^p + d{\sigma_{zz}}^p\right)\right] + \left[\dfrac{n_{xx}}{h+c}\left(d{\sigma_{xx}}^p n_{xx} + d{\sigma_{yy}}^p n_{yy} + d{\sigma_{zz}}^p n_{zz} + 2d{\tau_{xz}}^e n_{xz}\right)\right] = \\ \Psi\left\{\dfrac{1}{E}\left[d{\sigma_{xx}}^e - \vartheta\left(d{\sigma_{yy}}^p + d{\sigma_{zz}}^e\right)\right] + \left[\dfrac{n_{xx}}{h+c}\left(d{\sigma_{xx}}^e n_{xx} + d{\sigma_{yy}}^p n_{yy} + d{\sigma_{zz}}^e n_{zz} + 2d\tau_{xz}{}^e n_{xz}\right)\right]\right\} \\ d\varepsilon_{yy} = \dfrac{1}{E}\left[d{\sigma_{yy}}^p - \vartheta\left(d{\sigma_{xx}}^p + d{\sigma_{zz}}^p\right)\right] + \left[\dfrac{n_{yy}}{h+c}\left(d{\sigma_{xx}}^p n_{xx} + d{\sigma_{yy}}^p n_{yy} + d{\sigma_{zz}}^p n_{zz} + 2d{\tau_{xz}}^e n_{xz}\right)\right] = 0 \\ d{\sigma_{yy}}^p = \dfrac{1}{2}\left(d{\sigma_{xx}}^p + d{\sigma_{zz}}^p\right) \end{cases} \tag{7}$$

The other terms of above formula can be calculated

$$n_{ij}=\frac{S_{ij}-a_{ij}}{\sqrt{2k}},\ da_{ij}=cd\varepsilon_{ij}{}^{p},\ \Psi=1-\exp\left(-\kappa\frac{3h}{2G}\right),\ G=\frac{E}{2(1+\vartheta)} \tag{8}$$

where $h$ and is isotropic and kinematic hardening coefficients.

Our pilot experiemnts on processing of stainless steel 304 showed that the main contributed mechanisms on strengthening the surface layer after burnishing proess are formation of twinning and alpha ferrite. The next step after the calculation of the deformation parameter is to calculate the stress as results of twinning-induced hardening and phase changes.

Twinning-induced hardening.

The stress related to twining induced material strengthening has been presented in following equation [12]:

$$\begin{cases}\sigma_{TW}=M\beta_{TW}Gb\left(\dfrac{1}{d_{cell}}+\dfrac{1}{l}\right)\\ \dfrac{1}{l}=\dfrac{1}{2t}+\dfrac{f_{TW}}{1-f_{TW}}\end{cases} \tag{9}$$

where the $\sigma_{TW}$ is the term of strengthening stress as result of twinning, $M$ is Taylor factor, $\beta_{TW}$ is the constant, $t$ is the twin lamellae (that is 18nm) and $f_{TW}$ and is the twining volume fraction that is calculated by following differential equation:

$$df_{TW}=(1-f_{TW})A_f d\varepsilon \tag{10}$$

where $A_f$ is the constant that equals to 1.916 for twining induced plasticity austenitic stainless steels [13].

Phase change.

Transformation of austenite to ferrite usually occurs in cold working of austenitic stainless steel. The increasing rate of the ferrite during deformation is obtained by [14]:

$$f_m^{\bullet}=(1-f_m)v_m N_m^{\bullet} \tag{11}$$

where $f_m^{\bullet}$ is the rate of increase of ferrite volume fraction, $f_m$ is the ferrite volume fraction, $v_m$ is the average ferrite volume and $N_m^{\bullet}$ is the increase rate of ferrite that is related to its nucleation probability ($P$) on shear bands and the total number of ferrite nucleation ($N_I$).

$$N_m^{\bullet}=PN_I^{\bullet}+N_I P^{\bullet}H(P^{\bullet}) \tag{12}$$

where $H$ is Heaviside step function. Possible nucleation of ferrite is also affected by number of shear bands. Accordingly;

$$N_I^{\bullet}=\frac{rC\left(f_{sb}^{\bullet}\right)^{r-1}}{v_I},\ f_{sb}^{\bullet}=\alpha(1-f_{sb})\varepsilon^{\bullet} \tag{13}$$

where $r$ and $C$ are materials constant, $f_{sb}^{\bullet}$ is the increase rate of shear band volume fraction.

The ferrite nucleation probability was assumed to follow a Gaussian distribution,

$$P = \frac{1}{\sqrt{2\pi}\sigma_g} \int_{-\infty}^{g} \exp\left[ -\frac{1}{2}\left( \frac{g' - \bar{g}}{\sigma_g} \right)^2 \right] dg' \tag{14}$$

where the terms $\sigma_g$ and $\bar{g}$ are dimensionless mean and standard deviation, respectively. The thermodynamic driving force $g$ is related to the stress states ($\Sigma$) and the temperature ($T$), and is approximated by:

$$g = g_0 + g_1 T + g_2 \Sigma \tag{15}$$

where $g_0$, $g_1$, and $g_2$ are constants. A fraction function ($\chi$) of the plastic deformation is assumed cause temperature rise ($\Delta T$) as:

$$\Delta T = \int_0^{\varepsilon} \frac{\chi}{\rho C_p} \sigma(\varepsilon) d\varepsilon \tag{16}$$

where $\rho$ is material density and $C_P$ is the specific heat capacity.

As per the foresaid strain-induced phase transformation kinetics, the increase rate of the ferrite can then be obtained through combination of above-calculated equations:

$$\begin{cases} f_m^{\bullet} = (1 - f_m)\left( A\varepsilon^{\bullet} + B\Sigma^{\bullet} \right) \\ A = r\alpha\beta P (1 - f_{sb})(f_{sb})^{r-1} - B_f \dfrac{g_1 \chi}{\rho C_P} \sigma(\varepsilon) \qquad B = B_f g_2 \\ B_f = \dfrac{\beta}{\sqrt{2\pi}\sigma_g} (f_{sb})^r \exp\left[ -\dfrac{1}{2}\left( \dfrac{g' - \bar{g}}{\sigma_g} \right)^2 \right] H(P^{\bullet}) \\ \alpha = \alpha_0 + \alpha_1 T + \alpha_2 T^2 + \alpha_3 \Sigma \end{cases} \tag{17}$$

By identifying the ferrite volume fraction, the hardness development can be obtained as:

$$\Delta h = \sum_{i=1} f_i h_i - h_0 \tag{18}$$

where $f_i$ is the fraction of phase $i$ in the element, $h_0$ is the initial bulk microhardness, $h_i$ is the hardness of phase $i$, and $v$ represents the number of phases present in the element.

Accordingly, the final hardness of the sample after SSPD can be calculated by:

$$h = h_0 + k_D \sigma_D + k_{TW} \sigma_{TW} + \Delta h \tag{19}$$

**Experiments**

In the present investigation, surface sever plastic deformation experiments carried out by multi-roller rotary burnishing tool. The tool includes four rollers with diameter of 3mm and length of 10mm as shown in Fig. 2. The tool, as shown in the figure, has been mounted on a CNC milling machine to process the surface of the samples made of AISI 304. During the experiments, the burnishing force is controlled by a force dynamometer KISTLER 9257B as shown in Fig. 2. Samples were prepared in sizes of 70mm length, 30mm width and 10mm thickness. Before conducting the experiments, all the samples were milled with a same machining parameters to assure their flatness. The properties of the AISI 304, including the material's constitutive models,

i.e. Johnson-Cook, Isotropic-Kinematic hardening, dislocation density model, twinning-induced plasticity, and ferrite phase transformation constants, have been listed in Tables 1-4, respectively.

*Table 1. Johnson-Cook constants of AISI 304 [15].*

| $A$ (MPa) | $B$ (MPa | $C$ | $n$ |
|---|---|---|---|
| 452 | 694 | 0.0067 | 0.311 |

*Table 2. Isotropic-kinematic hardening constants of AISI 304 [15].*

| $h$ ( GPa ) | $c$ (GPa) |
|---|---|
| 2.7 | 0.8 |

*Table 3. Coefficients of austenite-ferrite phase change constitutive equation [14].*

| $\alpha_0$ | $\alpha_1$ | $\alpha_2$ | $\alpha_3$ | $g_0$ | $g_1$ | $g_2$ | $\beta$ |
|---|---|---|---|---|---|---|---|
| -2e- | 4.52e-2 | 11.8 | 0.8 | 0.05 | -1.2 | 78.3 | 4.5 |

The samples were mechanically polished on a suspension of ethylene glycol and diamond pastes with a gradation of 1 and 6μm. Then, they were electrolytically etched using a voltage of 12V and a exposure time of 30s in a solution of 10g CrO3 and 100 ml of distilled water. The microstructure was observed using a scanning electron microscope (SEM) JSM-IT200. The microhardness measurements were carried out using an Innovatest microhardness tester at a load of 0.245 N.

*Fig. 2. Experimental setup.*

A series of experiments was carried out to confirm the results obtained by the analytical models. Among the process factors, it was found that the burnishing depth has the most prominent effect on burnishing force and hardness. Thus, a total of three experiments under different burnishing

depths, i.e. 0.2mm, 0.25 mm, and 0.3mm were carried out, and the values of force and hardness distribution were taken into account to compare with the analytical model and understand the effect of factors on the hardening mechanism. During the experiments, spindle speed and feed rate were kept constant at 500 RPM and 200 mm/min, respectively. It needs to be pointed out that each experiment has been repeated three times, and the average values of performance measures (i.e., force and hardness) were reported in the paper.

**Results and Discussion**

In order to confirm the analytical model, the results of burnishing forces which were derived from the developed model was compared with those experimentally measured values. Fig. 3 demonstrates the comparison of measured and predicted values of burnishing axial force for the experimental data presented in Table 6. It is seen from the figure that there are good agreements between the measured and predicted values of burnishing force. According to the quantified results, the prediction errors vary between 5.2% and 8.7%. It can also be seen that the trend of variation of the main force with respect to process factors for those data calculated by the analytical model is well consistent with the experimental value. It is seen that, as a result of higher values of burnishing depth, the burnishing force increases. The higher value of burnishing depth increases the engagement radius and results in greater force.

Influence of burnishing depth on microhardness and influential parameters have been shown in Fig. 4. According to the figure, it is seen that for all three samples, there is close agreement between the measured and predicted values of microhardness. The error values are in the range of 14.3% to 21.5%, which seems acceptable based on the previous works carried out by different researchers [15]. Moreovr, it is clear in the figure that the microhardness hardness significantly increases by increasing the burnishing depth. This trend can be observed in both experimental results and modeled values. Therefore, the developed analytical model is accurate enough and can be utilized to find the influence of process factors on the microhardness.

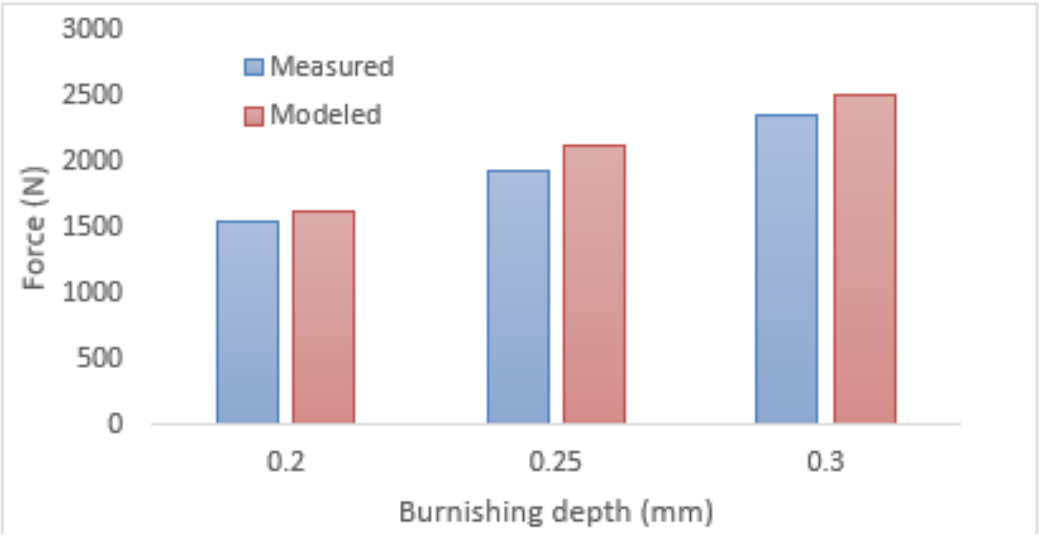


*Fig. 3. Comparison between measured and predicted values of burnishing force.*

As a result of increasing the burnishing depth, the burnishing axial force increases correspondingly (Fig. 3), which results in further values of plastic strain as shown in Fig. 5a. The greater value of plastic strain corresponds to a higher plastic strain rate under constant values of spindle speed and feed velocity, as shown in Fig. 5b. As result of further values of plastic strain and strain rate, the twinning volume fraction and ferrite volume fraction increase consequently as shown in Fig. 6a and 6b.

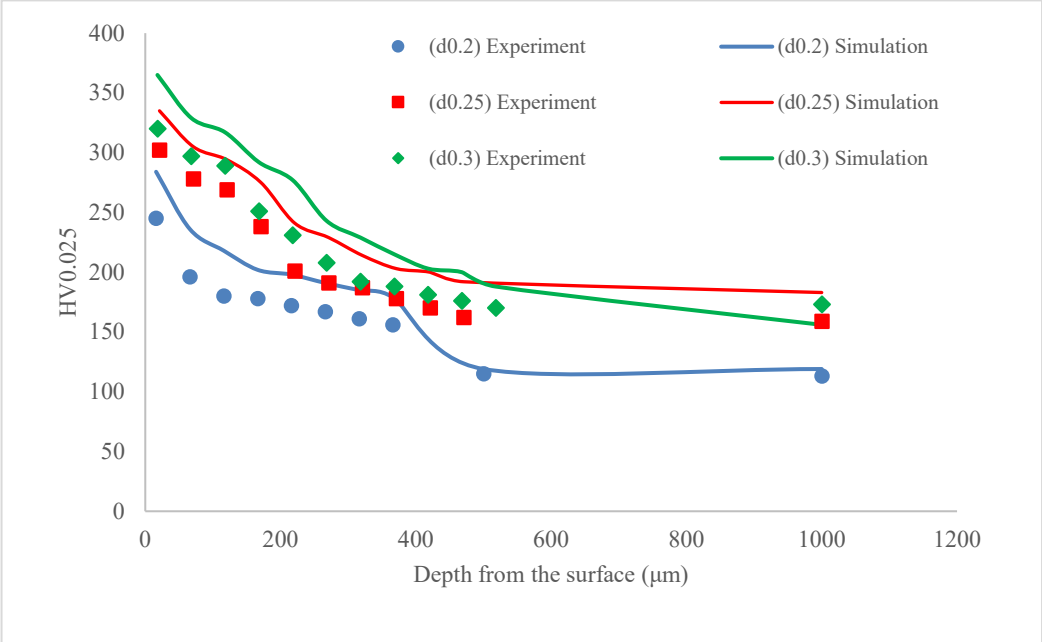


*Fig. 4. Comparison between measured and predicted values of microhardness.*

In order to check the results derived from the analytical model, scanning electron microscopic images of the surface and subsurface of the samples processed by burnishing at depths of 0.2 mm and 0.3 mm were captured and presented in Fig. 7. According to the figure, it is seen for the sample processed by 0.2mm burnishing depth, amount of twinning and ferrite contents which distributed in subsurface layers (as shown in Fig. 7a) are less than those of sample processed by burnishing depth of 0.3mm (as shown in Fig. 7b). It is seen that for the sample that was processed by further burnishing depth, the twinning, re-twinning, and ferrite content have been distributed up to the entire cross section of the sample that yields hardness development. It is also seen in Fig. 7a that in the deeper surface layer, the twinning induced hardening and austenite-ferrite phase change exist up to a certain depth, which can be considered a validation of the analytic model. This trend was predicted by the analytical model, where the twinning volume fraction is distributed at further depth (Fig. 6a), while the ferrite volume fraction is only available at a limited depth from the surface of the sample (Fig. 6b).

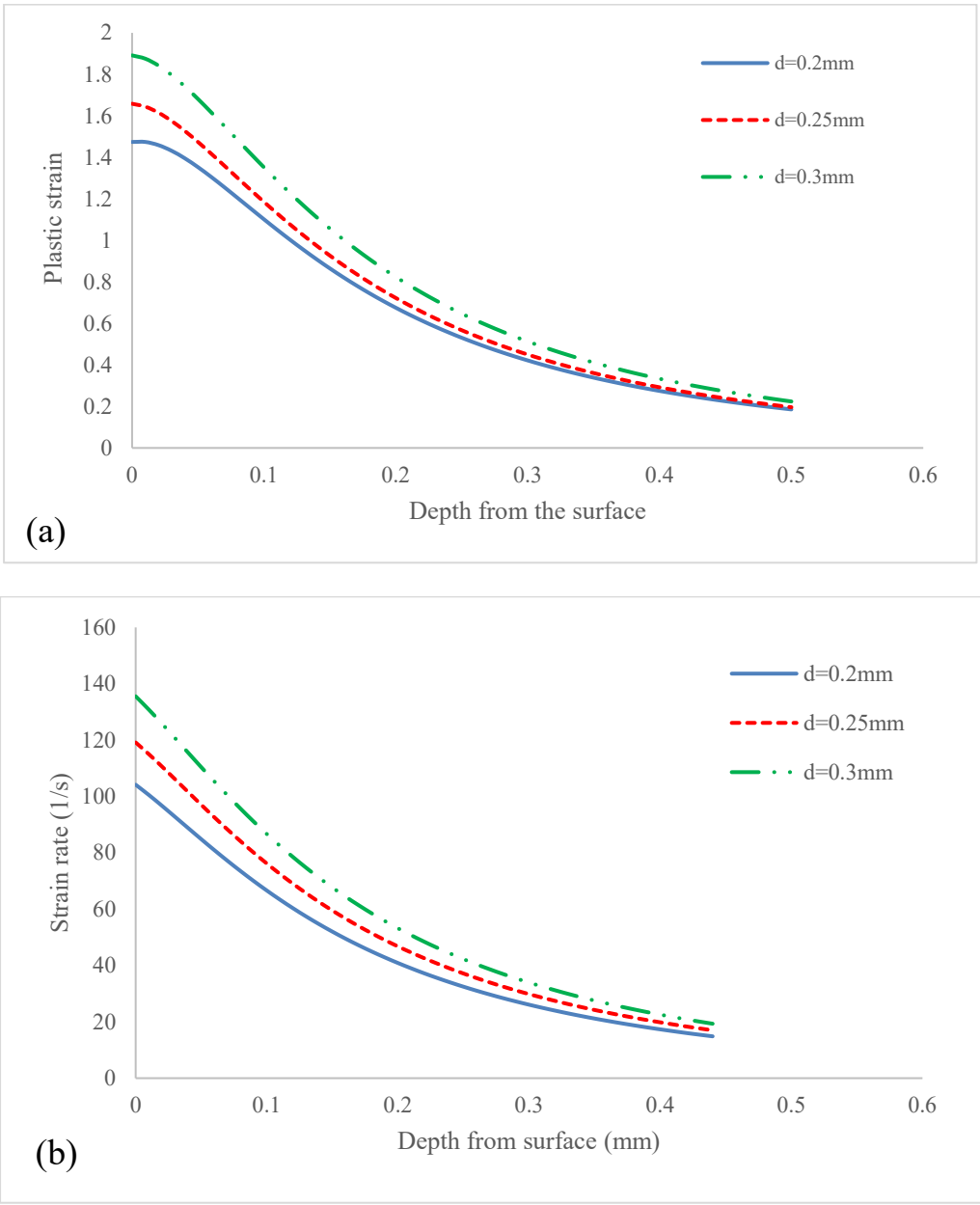


*Fig. 5. Effect of burnishing depth on (a) strain and (b) strain rate.*

**Summary**

The obtained results can be summarized as follows:

- There are close agreements between the measured and predicted values of burnishing force where the prediction error in worst case was around 9.1%. Moreover, microhardness distributions modeled by analytical approach were compatible with experiemental values where the maximum prediction error was 21.3%. Also, the trend of variations of hardness and burnishing force which were modeled by analytical approach were consistent well with experiemtnal findings.
- It was found that thanks to contributions of different hardening mechanisms, the micorhardness of the samples can be improved up to 200%. Among the different hardening mechanisms,

twinning-induced plasticity followed by phase change have the gretest effect on hardness development.

- It was found from the results that the phase change-induced hardening is only available in the layers very close to the surface e.g. 50μm in the best case; however, the twining volume fraction exists in much deeper surface layers.

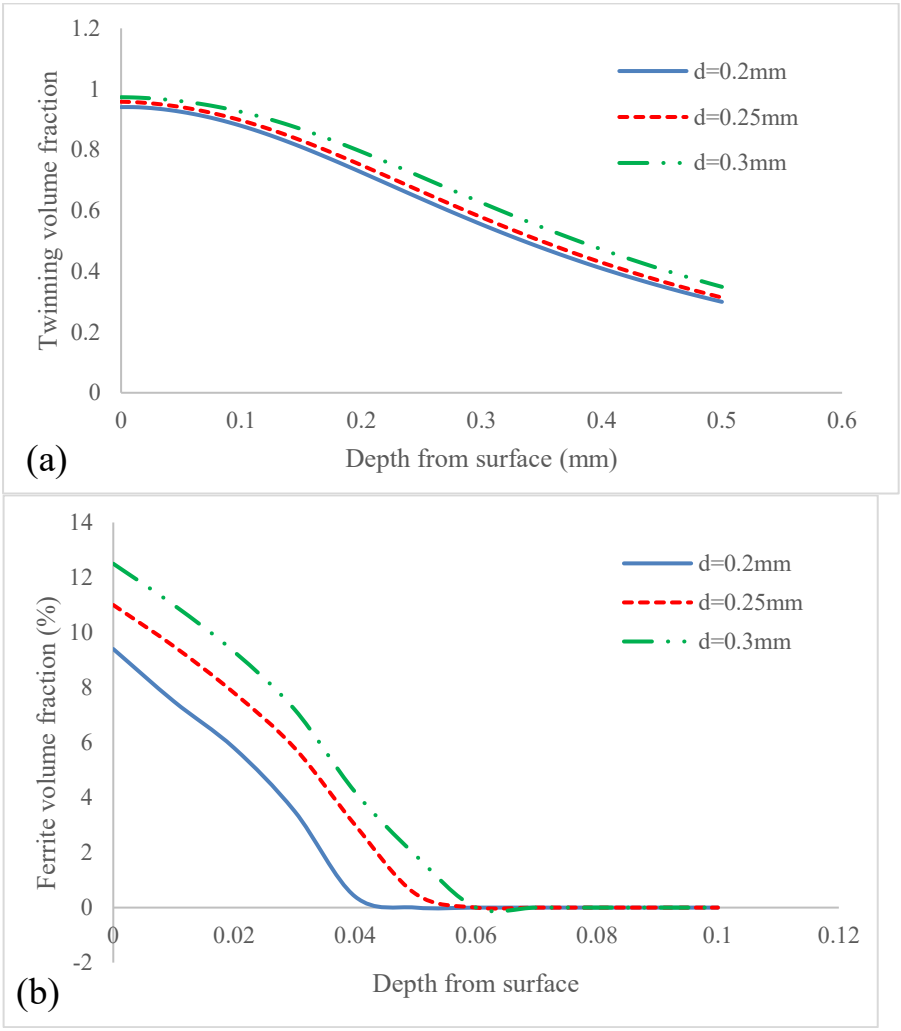


*Fig. 6. Effect of burnishing depth on (a) twinning volume fraction and (b) ferrite volume fraction.*

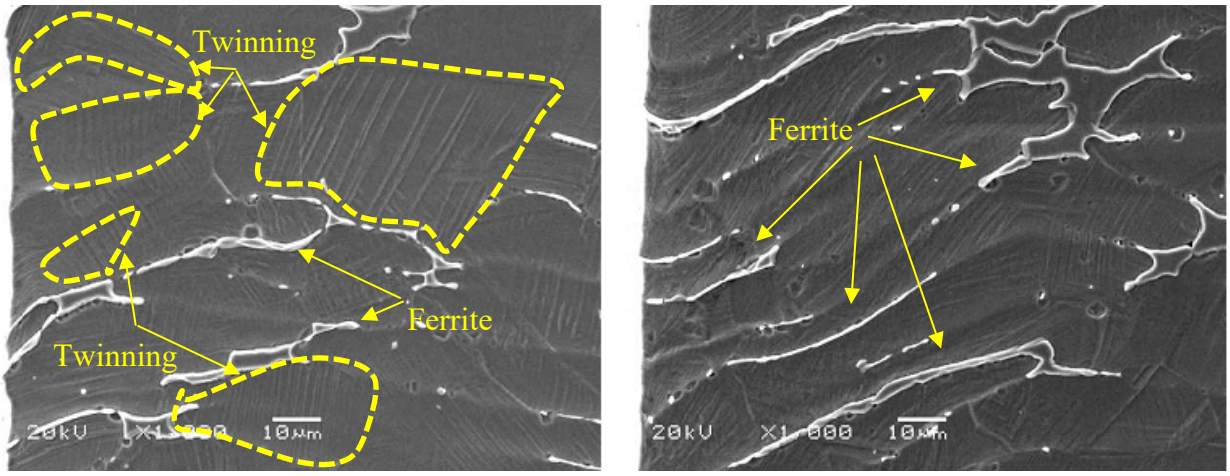


*Fig. 7. SEM image of cross section of near surface layers processed by different burnishing depth (a) 0.2mm (b) 0.3 mm (Spindle speed=500 RPM and feed velocity=200mm/min).*

**References**

[1] S. Attabi, A. Himour, L. Laouar, A. Motallebzadeh, Mechanical and wear behaviors of 316L stainless steel after ball burnishing treatment, J. Mat. Res. Tech. 15 (2021) 3255-3267. https://doi.org/10.1016/j.jmrt.2021.09.081

[2] Z.Y. Zhou, G.L. Yu, Q.Y. Zheng, G.Z. Ma, S.B. Ye, C. Ding, Z.Y. Piao, Wear behavior of 7075-aluminum after ultrasonic-assisted surface burnishing, J. Manuf. Process. 51 (2020) 1-9. https://doi.org/10.1016/j.jmapro.2020.01.026

[3] Y. Hua, Z. Liu, B. Wang, X. Hou, Surface modification through combination of finish turning with low plasticity burnishing and its effect on fatigue performance for Inconel 718, Surf. Coat. Technol. 375 (2019) 508-517. https://doi.org/10.1016/j.surfcoat.2019.07.057

[4] B. Starman, H. Hallberg, M. Wallin, M. Ristinmaa, M. Halilovič, Differences in phase transformation in laser peened and shot peened 304 austenitic steel, Int. J. Mech. Sci. 176 (2020) 105535. https://doi.org/10.1016/j.ijmecsci.2020.105535

[5] S.J. Lainé, K.M. Knowles, P.J. Doorbar, R.D. Cutts, D. Rugg, Microstructural characterisation of metallic shot peened and laser shock peened Ti–6Al–4V, Acta Mater. 123 (2017) 350-361. https://doi.org/10.1016/j.actamat.2016.10.044

[6] S. Rinaldi, D. Umbrello, S.N. Melkote, Modelling the effects of twinning and dislocation induced strengthening in orthogonal micro and macro cutting of commercially pure titanium, Int. J. Mech. Sci. 190 (2021) 106045. https://doi.org/10.1016/j.ijmecsci.2020.106045

[7] X.L. Gao, X.N. Jing, G. Subhash, Two new expanding cavity models for indentation deformations of elastic strain-hardening materials, Int. J. Solid Struct. 43 (2006) 2193-2208. https://doi.org/10.1016/j.ijsolstr.2005.03.062

[8] R. Teimouri, M. Grabowski, R. Bogucki, Ł. Ślusarczyk, S. Skoczypiec, Modeling of strengthening mechanisms of surface layers in burnishing process, Mater. Des. 223 (2022) 111114. https://doi.org/10.1016/j.matdes.2022.111114

[9] D.L. McDowell, G.J. Moyar, Effects of non-linear kinematic hardening on plastic deformation and residual stresses in rolling line contact, Wear 144 (1991) 19-37. https://doi.org/10.1016/0043-1648(91)90004-E

[10] K.L. Johnson, K.L. Johnson, Contact mechanics, Cambridge university press, 1987.

[11] Y. Liu, L. Wang, D. Wang, Finite element modeling of ultrasonic surface rolling process, J. Mater. Process. Technol. 211 (2011) 2106-2113. https://doi.org/10.1016/j.jmatprotec.2011.07.009

[12] F. Liu, W.J. Dan, W.G. Zhang, Strain hardening model of twinning induced plasticity steel at different temperatures, Mater. Des. 65 (2015) 737-742. https://doi.org/10.1016/j.matdes.2014.10.008
[13] G. Dini, R. Ueji, A. Najafizadeh, S.M. Monir-Vaghefi, Flow stress analysis of TWIP steel via the XRD measurement of dislocation density, Mater. Sci. Eng. A, 527 (2010) 2759-2763. https://doi.org/10.1016/j.matdes.2014.10.008
[14] W.J. Dan, W.G. Zhang, S.H. Li, Z.Q. Lin, A model for strain-induced martensitic transformation of TRIP steel with strain rate, Comput. Mater. Sci. 40 (2007) 101-107. https://doi.org/10.1016/j.commatsci.2006.11.006
[15] W. Zhang, X. Wang, Y. Hu, S.Wang, Predictive modelling of microstructure changes, micro-hardness and residual stress in machining of 304 austenitic stainless steel, Int. J. Mach. Tool. Manuf. 130 (2018) 36-48. https://doi.org/10.1016/j.ijmachtools.2018.03.008